VIP Metal–Organic Frameworks Very Important Paper

International Edition: DOI: 10.1002/anie.201504873
German Edition: DOI: 10.1002/ange.201504873

Morphological and Structural Evolutions of Metal–Organic Framework Particles from Amorphous Spheres to Crystalline Hexagonal Rods**

*Hee Jung Lee, Junghun We, Jun Oh Kim, Dooyoung Kim, Wonhee Cha, Eunji Lee, Jeungwon Sohn, and Moonhyun Oh**

Abstract: *Compositions as well as morphologies and structures of particles are vital factors that define their properties and applications. However, the morphology and structure changes associated with the composition change of metal–organic frameworks (MOFs) are barely studied. Herein, we report the morphology and structure changes of MOF particles associated with the ratio of two organic linkers incorporated within MOF particles, when they are constructed from the reactions of $In(NO_3)_3$ in the presence of isophthalic acid (H_2IPA) and/or 1,4-benzenedicarboxylic acid (H_2BDC). Two tendencies—the tendency of BDC and In^{3+} to form porous crystalline hexagonal rods, and the tendency of IPA and In^{3+} to form non-porous amorphous spherical particles—compete during the formation of MOF particles. Eventually, the incorporated ratio of BDC and IPA within the MOF particles, and thus their morphology and porosity, are controlled by altering the relative amounts of H_2BDC and H_2IPA used during the reactions.*

Micro- and nanoparticles constructed from atomic or molecular building blocks are of great interest because of their broad applications in catalysis, optics, sensing, and medical diagnostics.[1] Not only the compositions of micro- and nanoparticles, but also their morphologies and structures are important factors that define their properties and applications. Therefore, understanding changes in the morphology and structure of particles in response to change in the composition is critical for the controlled formation of particles. On the other hand, metal–organic frameworks (MOFs) or coordination polymers (CPs) have fascinating properties such as a high surface area, well-developed pores, and tunable compositions, and are therefore widely applied in gas storage, separation, catalysis, and sensing applications.[2] In these days, several micro- and nanosized MOFs and CPs have been developed for the production of advanced materials with enhanced properties and extended applications.[3] Moreover, MOF materials containing more than two kinds of metal ions or organic linkers have received a great deal of attention because they have extraordinary properties.[4] However, the morphological and structural changes related to the compositional change of MOFs have not been well studied. Herein, we report the interesting morphological and structural evolutions of MOFs according to the degree of contributions of two organic linkers, isophthalic acid (H_2IPA) and 1,4-benzenedicarboxylic acid (H_2BDC), during the MOF particle construction. Highly crystalline porous MOF particles were generated when the contribution of BDC linkers within the framework was dominant; however, amorphous non-porous MOF particles resulted when the contribution of the IPA linkers was superior. We also found that the resulting morphological feature of MOF particles as well as their porosity and structure were closely related to the relative amounts of the two organic linkers incorporated within MOF particles (Scheme 1).

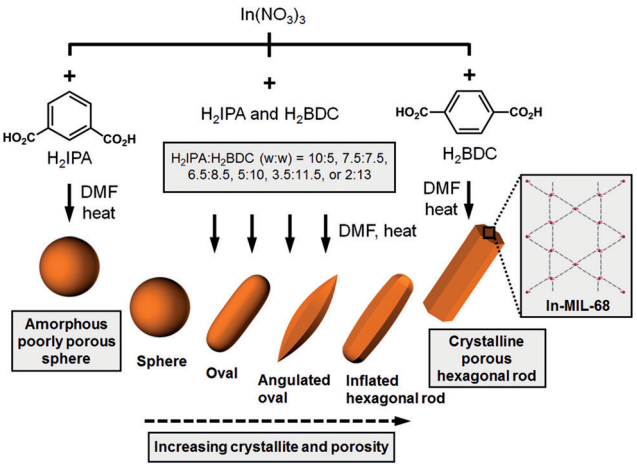

Scheme 1. Morphological evolution of MOF particles constructed from the solvothermal reactions of $In(NO_3)_3$ in the presence of H_2IPA and/or H_2BDC.

The solvothermal reaction of $In(NO_3)_3$ and H_2IPA in *N*,*N*-dimethylformamide (DMF) resulted in the formation of amorphous spherical particles with rough surfaces (Figure 1 a). However, crystalline hexagonal rods were generated from a similar reaction between $In(NO_3)_3$ and H_2BDC instead of H_2IPA (Figure 1 b), as reported before.[5] Such hexagonal rods are known to have a well-defined three-dimensional hexagonal structure of In-MIL-68.[6] However, we obtained a featureless powder X-ray diffraction (PXRD) pattern for spherical particles, indicating the formation of amorphous

[*] Dr. H. J. Lee, J. We, J. O. Kim, D. Kim, W. Cha, E. Lee, J. Sohn, Prof. M. Oh
Department of Chemistry, Yonsei University
50 Yonsei-ro, Seodaemun-gu, Seoul 120-749 (Korea)
E-mail: moh@yonsei.ac.kr

[**] This work was supported by a NRF grant funded by the Ministry of Science, ICT and Future Planning through the National Leading Research Lab Program (grant number NRF-2012R1A2A1A03670409).

Supporting information for this article is available on the WWW under http://dx.doi.org/10.1002/anie.201504873.

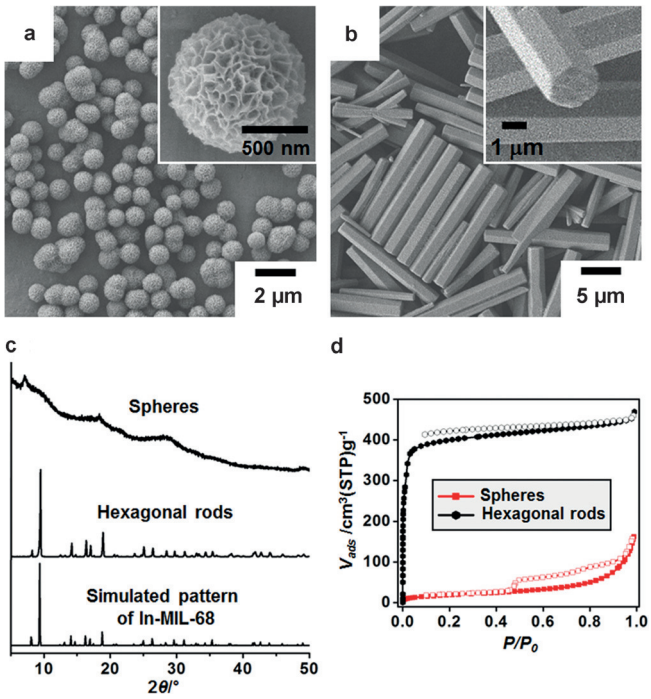

Figure 1. SEM images of a) spherical particles constructed from In^{3+} and H_2IPA, and b) hexagonal rods constructed from In^{3+} and H_2BDC. c) PXRD patterns of spherical particles (top), hexagonal rods (middle), and the simulated pattern of In-MIL-68 (bottom). d) N_2 sorption isotherms of spherical particles (red) and hexagonal rods (black) measured at 77 K. Solid symbols are adsorption and open symbols are desorption.

materials (Figure 1c). Infrared (IR) spectra of both spherical particles and hexagonal rods revealed the coordination of the carboxylate groups of IPA and BDC linkers to In^{3+}, as indicated by the characteristic shift of the CO stretching bands to 1609 and 1558 cm^{-1} after particle formation from 1693 and 1690 cm^{-1} for uncoordinated H_2IPA and H_2BDC, respectively (see Figure S1 in the Supporting Information). Hexagonal rods of In-MIL-68 constructed from $In(NO_3)_3$ and H_2BDC are known to be a quite porous material, as shown in N_2 sorption isotherms; however, the N_2 sorption isotherms of spherical particles constructed from $In(NO_3)_3$ and H_2IPA revealed the formation of poorly porous materials (Figure 1d). The Brunaure–Emmett–Teller (BET) surface area and total pore volume of the hexagonal rods were 1506 $m^2 g^{-1}$ and 0.73 $cm^3 g^{-1}$, respectively; however, the BET surface area and total pore volume of the spherical particles were only 69 $m^2 g^{-1}$ and 0.25 $cm^3 g^{-1}$, respectively.

Porous and crystalline hexagonal rods were constructed from the reaction of In^{3+} and H_2BDC, while poorly porous and amorphous spherical particles were generated from In^{3+} and H_2IPA. An additional curiosity on the morphological and structural changes of MOF particles associated with the incorporated ratio of the two organic linkers (H_2IPA and H_2BDC) within MOF particles prompted us to conduct further study. Within such a curiosity, a series of reactions in the presence of In^{3+} and various ratios of H_2IPA to H_2BDC have been carried out. First of all, the morphological evolution of MOF particles according to the ratio of the two organic linkers used during the reactions was monitored by scanning electron microscopy (SEM). In general, as the relative amount of H_2BDC used during the construction of MOF particles was increased from 33 to 87%, the morphology of MOF particles changed from spheres to ovals, angulated ovals, and finally almost hexagonal rods (Figure 2).

In detail, when a small amount of H_2BDC (5 mg) and a large amount of H_2IPA (10 mg) were used during the reaction, only spherical particles were produced (Figure 2a). Spherical particles may be produced because of the dominant contribution of IPA linkers during the construction of MOF particles. When the amount of H_2BDC used during the reaction was increased slightly to 7.5 mg and the amount of H_2IPA was reduced to 7.5 mg, a small proportion of oval-shaped MOF particles (designated as ovals) and a large proportion of spherical particles were produced (Figure 2b). The oval-shaped MOF particles become more abundant as the amount of H_2BDC used during the reaction was increased to 8.5 mg, as shown in Figure 2c. Furthermore, a dominant formation of oval-shaped MOF particles with well-angulated six facets (designated as angulated ovals) with a minor

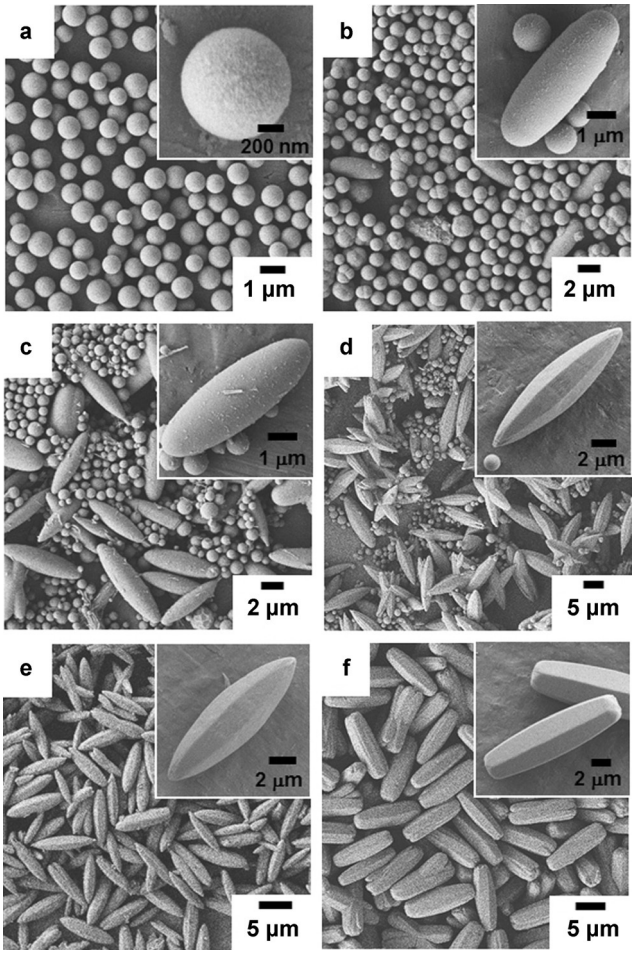

Figure 2. a–f) SEM images showing the morphological evolution of MOF particles constructed from the solvothermal reactions of $In(NO_3)_3$ in the presence of various ratios of H_2IPA and H_2BDC. The ratios of H_2IPA:H_2BDC (w:w) used during the reactions were (a) 10:5, (b) 7.5:7.5, (c) 6.5:8.5, (d) 5:10, (e) 3.5:11.5, and (f) 2:13.

formation of spherical particles occurred as the amount of H_2BDC was increased to 10 mg and the amount of H_2IPA was decreased to 5 mg (Figure 2d). When the amount of H_2BDC used was increased to 11.5 mg and the amount of H_2IPA used was decreased to 3.5 mg, angulated ovals were the only product (Figure 2e). Increasing contribution of BDC linkers within MOF particles possibly induce the formation of particles with morphology closer to hexagonal rods than spheres. Finally, when a very large amount of H_2BDC (13 mg) and a small amount of H_2IPA (2 mg) were used during the reaction, nearly hexagonal rods with a slightly inflated portion in the middle of rods were obtained (designated as inflated hexagonal rods, Figure 2f). Based on these results, we concluded that the morphology of intermediate MOF particles constructed from the reaction of In^{3+} in the presence of both H_2IPA and H_2BDC is dependent on the relative amounts of the two organic linkers used during the reactions. MOF particles constructed in the presence of large amounts of H_2BDC resembled hexagonal rods, because the dominant incorporation and significant contribution of BDC linkers were involved during the particle formation. However, MOF particles constructed in the presence of large amounts of H_2IPA resembled spherical particles because of the dominant contribution of IPA linkers in the particle formation.

The chemical compositions of a series of MOF particles were determined by energy dispersive X-ray (EDX) and ^1H NMR spectroscopy. First, EDX spectra of a series of MOF particles revealed that all products consisted of metal ions and organic linkers, as confirmed by detection of indium, carbon, and oxygen atoms (Figure S2). Second, the exact ratios of the amounts of both IPA and BDC linkers incorporated within particles were determined by ^1H NMR spectra of the digested MOF particles in [D_4]acetic acid and [D_6]DMSO (Figure 3). The ratio of IPA and BDC linkers within the inflated hexagonal rods was determined to be 1:5.76 by integrating the peaks in the spectrum (Figure 3f). It should be remained

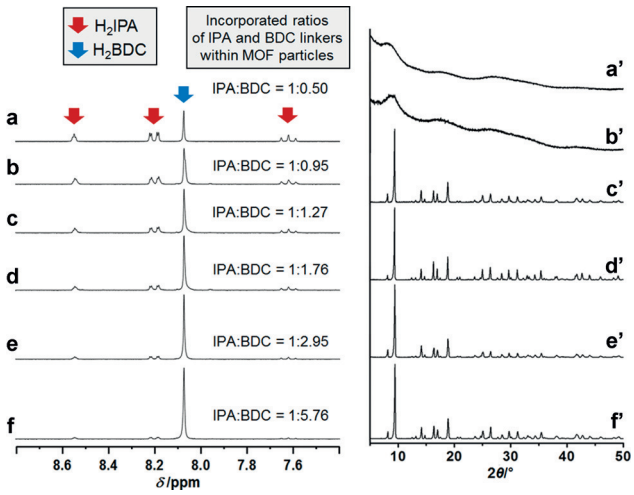

Figure 3. a–f) ^1H NMR spectra of differently shaped MOF particles digested in [D_4]acetic acid and [D_6]DMSO. The ratios of H_2IPA:H_2BDC (w:w) used during the reactions to construct MOF particles were a) 10:5, b) 7.5:7.5, c) 6.5:8.5, d) 5:10, e) 3.5:11.5, and f) 2:13. a′–f′) PXRD patterns of MOF particles.

that the inflated hexagonal rods were constructed from the reaction of In^{3+} in the presence of 1:6.5 of H_2IPA:H_2BDC (w:w). The relative amount of IPA to BDC within the angulated ovals was 1:2.95 (Figure 3e) when these particles were constructed in the presence of 1:3.29 of H_2IPA:H_2BDC. ^1H NMR spectra of the digested spherical particles constructed from the reaction of In^{3+} and 1:0.5 of H_2IPA:H_2BDC revealed that they consisted of 1:0.5 of IPA:BDC (Figure 3a). These results indicated that the relative amounts of IPA and BDC linkers incorporated within MOF particles were fairly consistent with those of H_2IPA and H_2BDC used during the reactions, as shown in Figure 3.

The PXRD patterns of inflated hexagonal rods (Figure 3f′), angulated ovals (Figure 3e′,d′), and ovals (Figure 3c′) were almost identical to those of pure hexagonal rods of In-MIL-68. Even though IPA linkers in addition to BDC linkers were present in MOF particles, MOF particles constructed from the dominant contribution of BDC linkers, such as inflated hexagonal rods, angulated ovals, and ovals, were highly crystalline materials that had a three-dimensional hexagonal structure similar to that of pure In-MIL-68. However, spherical particles (Figure 3a′), which contained a relatively high proportion of IPA linkers, had amorphous characteristic similar to particles produced from pure IPA linkers. Based on these results, we concluded that highly crystalline MOF particles were produced when the contribution of BDC linkers to MOF particles increased, while amorphous MOF particles were obtained when the contribution of IPA linkers to MOF particles increased. A plausible reason for the structural transition from crystalline to amorphous can be found from the different degree of disorders of the two organic linkers. Many possible disorders of IPA linkers within the MOF structure likely resulted in the formation of amorphous materials during the rapid synthesis of MOF particles. Several crystalline MOFs containing IPA linkers have been reported;[7] however, these crystalline MOFs were usually constructed slowly to ensure sufficient time for the construction of a well-ordered crystalline structure.

The porosities of a series of MOF particles were obtained from their N_2 sorption isotherms. In general, the BET surface areas and total pore volumes of MOF particles increased with increasing the amounts of BDC linkers incorporated within MOF particles, thereby increasing the contribution of BDC linkers within the framework (Figure 4). Hexagonal rods constructed from In^{3+} and pure H_2BDC were highly porous, while spherical particles constructed from In^{3+} and pure H_2IPA were almost non-porous (Figure 1d). In detail, spherical MOF particles (see Figure 2a) consisting of 1:0.50 of IPA:BDC were non-porous materials ($12\ m^2\ g^{-1}$ and $0.03\ cm^3\ g^{-1}$) while the BET surface area and total pore volume ($79\ m^2\ g^{-1}$ and $0.12\ cm^3\ g^{-1}$) of products containing a major proportion of spherical particles with a minor proportion of ovals (see Figure 2b) were slightly higher than those of spherical particles because of the contribution from small amounts of oval particles. As the contribution of BDC linkers within MOF particles increased, the BET surface areas and total pore volumes of MOF particles steadily increased (Figure 4). The BET surface areas and total

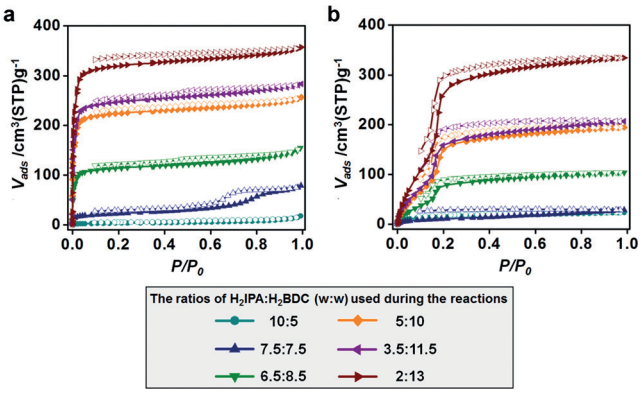

Figure 4. a) N_2 sorption isotherms measured at 77 K and b) CO_2 sorption isotherms measured at 195 K of differently shaped MOF particles constructed from the reactions of $In(NO_3)_3$ in the presence of various ratios of H_2IPA and H_2BDC. The ratios of H_2IPA:H_2BDC (w:w) used during the reactions were 10:5 (cyan), 7.5:7.5 (blue), 6.5:8.5 (green), 5:10 (orange), 3.5:11.5 (purple), and 2:13 (brown). Solid symbols are adsorption and open symbols are desorption.

pore volumes (860 $m^2 g^{-1}$ and 0.40 $cm^3 g^{-1}$) of the mixture of angulated ovals and small amounts of spherical particles (see Figure 2d) were slightly lower than those (933 $m^2 g^{-1}$ and 0.44 $cm^3 g^{-1}$) of pure angulated ovals (see Figure 2e) because of the small contribution of non-porous spherical particles. The values for BET surface areas and total pore volume (1208 $m^2 g^{-1}$ and 0.55 $cm^3 g^{-1}$) of inflated hexagonal rods (see Figure 2f) located between those of pure hexagonal rods and angulated ovals. Pore size distributions of a series of the resulting MOF particles were calculated using the non-local density functional theory (NLDFT) method (Figure S3). CO_2 sorption isotherms of MOF particles were also measured at 195 K (Figure 4b). The trend of the CO_2 uptake ability of a series of MOF particles was similar to that of their N_2 sorption properties. Overall, there was competition between the tendency of BDC linker and In^{3+} to form crystalline, porous, and angulated hexagonal rods, and the tendency of IPA linker and In^{3+} to form amorphous, non-porous, and unangulated spherical particles. The incorporated ratio of these two linkers within MOF particles determined the morphological and structural features of the resulting MOF particles.

In conclusion, we have characterized the morphological and structural evolutions of MOF particles driven by different degrees of contribution of the two organic linkers (H_2BDC and H_2IPA) during the MOF particle construction. Highly porous hexagonal rods with a well-developed, three-dimensional hexagonal structure were generated from the reaction of In^{3+} and H_2BDC; however, poorly porous spherical particles with amorphous features were produced from the reaction of In^{3+} and H_2IPA. The morphological features of MOF particles constructed from the reactions of In^{3+} in the presence of both H_2BDC and H_2IPA located somewhere between hexagonal rods and spheres. Specifically, MOF particles constructed from a relatively large amount of BDC linkers and a small amount of IPA linkers resembled a hexagonal rod, while MOF particles created from a relatively small amount of BDC linkers and a large amount of IPA linkers were close to a sphere. The porosities of the resulting MOF particles increased steadily as the contribution of BDC linkers within MOF particles increased. The incorporated ratio of BDC and IPA linkers within MOF particles, and thus the morphology and porosity of particles, were controlled by changing the relative amounts of H_2BDC and H_2IPA used during the reactions.

Keywords: hybrid materials · metal–organic frameworks · microparticles · morphological evolutions · porosity

How to cite: *Angew. Chem. Int. Ed.* **2015**, *54*, 10564–10568
Angew. Chem. **2015**, *127*, 10710–10714

[1] a) D. Astruc, F. Lu, J. R. Aranzaes, *Angew. Chem. Int. Ed.* **2005**, *44*, 7852–7872; *Angew. Chem.* **2005**, *117*, 8062–8083; b) Q. Zhang, X.-Z. Shu, J. M. Lucas, F. D. Toste, G. A. Somorjai, A. P. Alivisatos, *Nano Lett.* **2014**, *14*, 379–383; c) M. Oh, C. A. Mirkin, *Nature* **2005**, *438*, 651–654; d) Y. Nakayama, P. J. Pauzauskie, A. Radenovic, R. M. Onorato, R. J. Saykally, J. Liphardt, P. Yang, *Nature* **2007**, *447*, 1098–1101; e) J. I. L. Chen, Y. Chen, D. S. Ginger, *J. Am. Chem. Soc.* **2010**, *132*, 9600–9601; f) F. Wang, Y. Han, C. S. Lim, Y. Lu, J. Wang, J. Xu, H. Chen, C. Zhang, M. Hong, X. Liu, *Nature* **2010**, *463*, 1061–1065; g) K. Saha, S. S. Agasti, C. Kim, X. Li, V. M. Rotello, *Chem. Rev.* **2012**, *112*, 2739–2779; h) D. A. Giljohann, D. S. Seferos, W. L. Daniel, M. D. Massich, P. C. Patel, C. A. Mirkin, *Angew. Chem. Int. Ed.* **2010**, *49*, 3280–3294; *Angew. Chem.* **2010**, *122*, 3352–3366; i) Y.-w. Jun, J.-H. Lee, J. Cheon, *Angew. Chem. Int. Ed.* **2008**, *47*, 5122–5135; *Angew. Chem.* **2008**, *120*, 5200–5213.

[2] a) A. Phan, C. J. Doonan, F. J. Uribe-Romo, C. B. Knobler, M. O'Keeffe, O. M. Yaghi, *Acc. Chem. Res.* **2010**, *43*, 58–67; b) Y. He, W. Zhou, G. Qian, B. Chen, *Chem. Soc. Rev.* **2014**, *43*, 5657–5678; c) J. An, S. J. Geib, N. L. Rosi, *J. Am. Chem. Soc.* **2010**, *132*, 38–39; d) O. K. Farha, A. Ö. Yazaydın, I. Eryazici, C. D. Malliakas, B. G. Hauser, M. G. Kanatzidis, S. T. Nguyen, R. Q. Snurr, J. T. Hupp, *Nat. Chem.* **2010**, *2*, 944–948; e) K. Sumida, D. L. Rogow, J. A. Mason, T. M. McDonald, E. D. Bloch, Z. R. Herm, T.-H. Bae, J. R. Long, *Chem. Rev.* **2012**, *112*, 724–781; f) H. Fei, S. M. Cohen, *J. Am. Chem. Soc.* **2015**, *137*, 2191–2194; g) X. Gu, Z.-H. Lu, H.-L. Jiang, T. Akita, Q. Xu, *J. Am. Chem. Soc.* **2011**, *133*, 11822–11825; h) O. Kozachuk, I. Luz, F. X. Llabrés i Xamena, H. Noei, M. Kauer, H. B. Albada, E. D. Bloch, B. Marler, Y. Wang, M. Muhler, R. A. Fischer, *Angew. Chem. Int. Ed.* **2014**, *53*, 7058–7062; *Angew. Chem.* **2014**, *126*, 7178–7182; i) L. E. Kreno, K. Leong, O. K. Farha, M. Allendorf, R. P. Van Duyne, J. T. Hupp, *Chem. Rev.* **2012**, *112*, 1105–1125; j) W. Cho, H. J. Lee, G. Choi, S. Choi, M. Oh, *J. Am. Chem. Soc.* **2014**, *136*, 12201–12204; k) Y. Guo, X. Feng, T. Han, S. Wang, Z. Lin, Y. Dong, B. Wang, *J. Am. Chem. Soc.* **2014**, *136*, 15485–15488.

[3] a) P. Horcajada, T. Chalati, C. Serre, B. Gillet, C. Sebrie, T. Baati, J. F. Eubank, D. Heurtaux, P. Clayette, C. Kreuz, J.-S. Chang, Y. K. Hwang, V. Marsaud, P.-N. Bories, L. Cynober, S. Gil, G. Férey, P. Couvreur, R. Gref, *Nat. Mater.* **2010**, *9*, 172–178; b) J. Della Rocca, D. Liu, W. Lin, *Acc. Chem. Res.* **2011**, *44*, 957–968; c) S. Jung, W. Cho, H. J. Lee, M. Oh, *Angew. Chem. Int. Ed.* **2009**, *48*, 1459–1462; *Angew. Chem.* **2009**, *121*, 1487–1490; d) A. Foucault-Collet, K. A. Gogick, K. A. White, S. Villette, A. Pallier, G. Collet, C. Kieda, T. Li, S. J. Geib, N. L. Rosi, S. Petoud, *Proc. Natl. Acad. Sci. USA* **2013**, *110*, 17199–17204; e) D. Tanaka, A. Henke, K. Albrecht, M. Moeller, K. Nakagawa, S. Kitagawa, J. Groll, *Nat. Chem.* **2010**, *2*, 410–416; f) M. Pang, A. J. Cairns, Y. Liu, Y. Belmabkhout, H. C. Zeng, M. Eddaoudi, *J. Am. Chem. Soc.* **2012**, *134*, 13176–13179; g) Z. Zhang, Y. Chen, X. Xu, J. Zhang, G. Xiang, W. He, X. Wang, *Angew. Chem. Int. Ed.* **2014**, *53*, 429–433; *Angew. Chem.* **2014**, *126*, 439–443; h) S. Xu, L. You, P. Zhang, Y. Zhang, J. Guo, C. Wang, *Chem. Commun.* **2013**, *49*, 2427–2429.

[4] a) H. Furukawa, U. Müller, O. M. Yaghi, *Angew. Chem. Int. Ed.* **2015**, *54*, 3417 – 3430; *Angew. Chem.* **2015**, *127*, 3480 – 3494; b) K. Hirai, S. Furukawa, M. Kondo, H. Uehara, O. Sakata, S. Kitagawa, *Angew. Chem. Int. Ed.* **2011**, *50*, 8057 – 8061; *Angew. Chem.* **2011**, *123*, 8207 – 8211; c) H. J. Lee, Y. J. Cho, W. Cho, M. Oh, *ACS Nano* **2013**, *7*, 491 – 499; d) H. J. Lee, K. Lee, W. Cho, Y. J. Cho, M. Oh, *CrystEngComm* **2012**, *14*, 2837 – 2842.

[5] W. Cho, H. J. Lee, M. Oh, *J. Am. Chem. Soc.* **2008**, *130*, 16943 – 16946.

[6] C. Volkringer, M. Meddouri, T. Loiseau, N. Guillou, J. Marrot, G. Férey, M. Haouas, F. Taulelle, N. Audebrand, M. Latroche, *Inorg. Chem.* **2008**, *47*, 11892 – 11901.

[7] a) J. Gao, K. Ye, M. He, W.-W. Xiong, W. Cao, Z. Y. Lee, Y. Wang, T. Wu, F. Huo, X. Liu, Q. Zhang, *J. Solid State Chem.* **2013**, *206*, 27 – 31; b) A. M. Kirillov, Y. Y. Karabach, M. Haukka, M. F. C. Guedes da Silva, J. Sanchiz, M. N. Kopylovich, A. J. L. Pombeiro, *Inorg. Chem.* **2008**, *47*, 162 – 175; c) C. Zhang, M. Zhang, L. Qin, H. Zheng, *Cryst. Growth Des.* **2014**, *14*, 491 – 499.

Received: May 29, 2015
Published online: July 14, 2015

